13th International Symposium on Turbulence and Shear Flow Phenomena (TSFP13)
Montreal, Canada, June 25–28, 2024

ANISOTROPIC DAMPING OF STEADY AND PULSATILE SHEAR LAYERS IN TURBULENT SHEAR-THINNING FLOWS

Moira Barnes[1]
[1]Dept. of Mechanical and Materials Eng.
Queen's University
Kingston, Ontario, Canada
moira.barnes@queensu.ca

Giuseppe A. Rosi[2]
[2]Institute of Fluid Mechanics
Technische Universität Braunschweig
Braunschweig, Niedersachsen, Germany
giuseppe-antonio.rosi@tu-braunschweig.de

David E. Rival[1,2]
[2]Institute of Fluid Mechanics
Technische Universität Braunschweig
Braunschweig, Niedersachsen, Germany
david.rival@tu-braunschweig.de

ABSTRACT

Previous studies have observed that shear-thinning fluids attenuate fluctuations normal to the direction of primary fluid shear. This anisotropic attenuation would suggest that a shear layer forming within a shear-thinning fluid would be have reduced turbulent fluctuations when compared to a shear layer forming within a Newtonian fluid for the same equivalent Reynolds number. It is hypothesized that these anisotropic effects in shear-thinning fluids will culminate in steady and unsteady turbulent shear layers that exhibit consistent large-scale flow topologies and other large-scale quantifiable metrics, but whose small-scale structures exhibit attenuation. To test the hypothesis, this study investigates vortical structures generated from steady and pulsatile shear layers within shear-thinning fluids of varying shear-thinning strength. Shear layers were generated using a sudden expansion and the resultant flow fields were captured using particle image velocimetry. Tested fluids exhibited approximate power-law indices of 1, 0.81, 0.61 and 0.47. All flow measurements were performed at mean, throat-based, effective Reynolds numbers of $\mathrm{Re_m} = 4800$ and 14400, while the pulsatile flows were tested at a Strouhal number and a pulsatile velocity amplitude ratio of $\mathrm{St} = 0.15$ and $\lambda = 0.95$, respectively. If the anisotropic fluctuation damping of shear-thinning fluids is negligible, then no disparities should manifest between test cases of equal Reynolds number. Clear evidence of anisotropic behaviour in the shear layer was not found in time- or phase-averaged quantities, demonstrated by the circulation for the unsteady shear layers and by the vorticity thickness for the steady shear layers. However, enstrophy fields for the unsteady shear layers and vorticity and Reynolds shear-stress spectra of the steady shear layers reveal anisotropic behaviour not captured by the Reynolds number, specifically increased small-scale vortical-structure attenuation; and increased diffusion of Kelvin-Helmholtz instabilities with increasing shear-thinning strength. Instabilities also frequently coalesce into large rollers within the steady shear layers, an occurrence thought to be promoted by increased stability produced by the molecular structure of the shear-thinning agent.

INTRODUCTION

There are a myriad of situations that involve unsteady and rotational flow of shear-thinning fluids. Consider, for example, cardiovascular flow in which blood, a shear-thinning fluid (Lin *et al.*, 2014), exits the left ventricle and into the ascending aorta at varying degrees of unsteadiness. Depending on a person's level of activity, the unsteady blood flow can display turbulence (Sundin *et al.*, 2022). Flows with unsteadiness and flow separation will necessarily be dominated by vortical structures. However, although the presence of such vortical structures have been studied in flows involving Newtonian fluids (Hussain 1986), the nature of such structures remains relatively unexplored for shear-thinning flows.

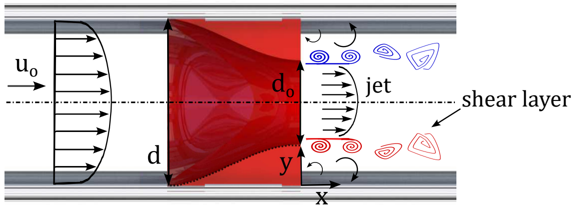

(a) steady

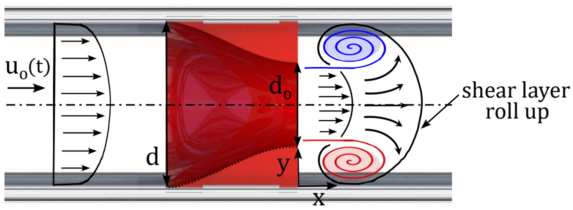

(b) unsteady

Figure 1: (a) As fluid flows through a pipe at velocity of u_m, the flow is gradually contracted to a throat diameter of d_o, where it is expanded, resulting in shed vortical structures being convected downstream along the shear layer. (b) In pulsatile cases, fluid pulses about a mean velocity of u_m at a frequency of f, inducing shear-layer roll up with small-scale instabilities embedded within the large-scale vortical structure. The pulsatile flows can be described by the Strouhal number $\mathrm{St} = f d_\mathrm{o}/u_\mathrm{m}$.

Modeling of turbulent shear-thinning flows in complex geometries often requires the application of a laminar molecular viscosity fit, often in the form of the power law, the Cross model, the Carreau-Yasuda or Hershel-Bulkely fit (Kelessidis *et al.*, 2011). All of the models reduce viscosity with increased strain rate, suggesting a tendency for shear-thinning fluids to always augment turbulence in the presence of increased shear. However, simulations of turbulent shear-thinning flows focused on canonical cases such as steady pipe or channel flow have shown that increasing shear-thinning strength results in a dampening of turbulence when compared to Newtonian counterparts (Terrapon *et al.*, 2004; White & Mungal, 2008; Rudman *et al.*, 2004). The mechanism behind this turbulent dampening and the resultant reduction in drag is believed to arise from the complex polymer chain extension process and subsequent attenuation of near-wall turbulence regeneration (Mrokowska & Krzton-Maziopa, 2019; Terrapon *et al.*, 2004). Additionally, it has been shown that similar bulk-viscosity models are unable to capture complex vortex-ring formation in dense suspension flows (Zhang & Rival, 2020).

According to bulk-viscosity models, a shear-thinning fluid and a Newtonian fluid should quantitatively and topologically result in the same flow field so long as the flows are geometrically similar and share the same Reynolds number. However, increasing shear-thinning strength has been shown to result in a dampening of turbulence when compared to Newtonian counterparts (Terrapon *et al.*, 2004; White & Mungal, 2008; Rudman *et al.*, 2004). To investigate the contradictory results of applying an effective Reynolds number using a bulk-viscosity model, the current study considers the formation of steady and unsteady shear layers behind an axisymmetric expansion, an environment in which the shear-layer formation within Newtonian fluids is documented, allowing for shear-thinning strength effects to be assessed through comparison. Typical scales of coherent structures formed downstream of a sudden expansion in steady and pulsatile flows are shown in Figure 1.

In this study, unsteady shear layers can be made analogous to a vortex ring formed by an upstream pulsed flow with a formation time of $T^* = 1/\mathrm{St}$ (Dabiri, 2009). The formation time is roughly equal to $3.6 \leq T^* \leq 4.5$, at which point the vortex ring accepts the maximum flux of rotational fluid from the shear layer before pinch-off (Gharib *et al.*, 1998). As Reynolds number increases to transitional and turbulent regime in Newtonian fluids, increased radial instabilities occur where vorticity stretching and tilting should cause reduced relative in-plane circulation (Glezer, 1988). However, as previously mentioned, shear-thinning fluids exhibit a dampening of turbulence, which could potentially mitigate these out-of-plane instabilities. With regards to shear-thinning fluids, studies have shown that the formation of isolated laminar vortex rings is somewhat affected by the fluid's shear-thinning strength with reduced circulation rates as shear-thinning strength increases. However, shear-thinning strength has been shown to have no effect on the subsequent evolution and breakdown of the vortex (Bentata *et al.*, 2018; Palacios-Morales & Zenit, 2013). Comparatively, steady shear flows of turbulent shear-thinning fluid have demonstrated strong anisotropic behaviour with dampening in the spanwise direction (Escudier *et al.*, 2009). Furthermore, in simulations by Kumar & Homsy (1999), a fluid's shear-thinning strength was shown to inhibit small-scale structures such as shear-layer instabilities in steady flows, namely the Kelvin-Helmholtz (KH) instability.

Based on the results of the aforementioned studies, it is hypothesized that these anisotropic effects in shear-thinning fluids will culminate in steady and unsteady turbulent shear layers that exhibit consistent large-scale flow topologies and other large-scale quantifiable metrics, but whose small-scale structures exhibit attenuation. This experiment will investigate this hypothesis by examining a range of pulsatile and steady flows with increasing shear-thinning strength.

EXPERIMENTAL METHODS

In this study, vortical structures are generated by the pulsatile operation of a flow loop. The flow loop possesses a section made of acrylic pipe, which allows optical access. A general sudden expansion model is placed within the acrylic pipe, reducing the inner diameter from $d = 76.2$mm to $d_\mathrm{o} = 38.1$mm, resulting in a diameter ratio of 0.5. The sudden expansion model creates separated flow that induces vortical structures and has previously been used to study separated flows and mixing in pulsatile, dense-suspension flows (Jeronimo & Rival 2021). The axisymmetric sudden expansion is described by the smooth curve $y(x) = \frac{1}{2}\left[d_\mathrm{o} + (d - d_\mathrm{o})\sin^2\left(\frac{\pi x}{2L}\right)\right]$ for $-0.5 \leq x/L \leq 0$, where x is the position along the acrylic pipe and $L = 7.6$ cm is the length of the installed axisymmetric sudden expansion. The working fluids in this experiment are produced and stored in a 341L reservoir from which the fluid is pumped using a programmable circumferential piston pump (Viking Pumps, Cedar Falls, US). The flow pattern and rate are controlled by sending analogue signals using LabView (National Instruments, Austin, US), and a digital acquisition device (National Instruments, Austin, US). The experimental setup can be seen in Figure 2.

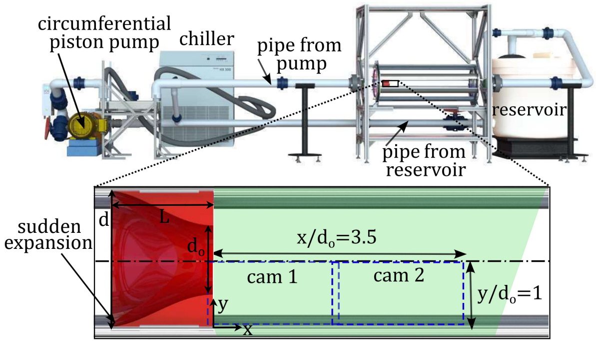

Figure 2: Experimental setup of sudden expansion, with the laser-light sheet depicted in green. The total field-of-view extends downstream from the outlet of the sudden expansion $3.5d_\mathrm{o}$ and vertically $1.0d_\mathrm{o}$ from the bottom of the acrylic pipe.

Two-dimensional particle image velocimetry (2D-PIV) was carried out on various fluids that were seeded with 9–13μm diameter hollow glass spheres (LaVision 1108952). Two high-speed cameras (Photonics PA4) were used, with f = 62mm lenses (Nikon). These cameras were placed to image the flow exiting the sudden expansion and together captured a $3.5d_\mathrm{o} \times 1.0d_\mathrm{o}$ field-of-view. The setup can be seen in Figure 2. A 65 mJ-per-pulse high-speed laser (Photonics DM60-527) was used to create a thin laser sheet. The laser pulse was synced with the cameras allowing time-resolved images to be captured. To evaluate flow fields, cross-correlation methods were applied using DaVis 8.4.0 (Lavision, Gottingen, Germany) using a multipass overlapping window technique, with 50% overlap and 24×24 pixel final window size. In post-processing, correlation peak validation, median test, and interpolation are used. The resulting spatial resolution is approximately 0.8×0.8mm.

The working fluids used in this study consist of solutions of xanthan gum (Dunkirken Foods, Summerside, Canada) prepared using 35 parts per million (PPM), 450PPM and 900PPM of xanthan gum and water. Fluids are characterized using both concentric-cylinder and cone-plate style rheometers (Palacios-Morales & Zenit 2013; Rahgozar & Rival 2017). All working fluids are approximated as power-law fluids in the form of $\mu = k\gamma^{n-1}$. The power-law index n, which reduces with increasing shear-thinning strength of a fluid, was found to be 0.81, 0.61, and 0.48 for 35PPM, 450PPM, and 900PPM respectively. The reduction in viscosity with increasing strain rate is shown in Figure 3 for all fluids, accompanied by a typical blood analogue for comparison (Lin *et al.* 2014).

The effect of increasing a fluid's shear-thinning strength on the formation and development of the shear layer and vortical structures is investigated across various mean Reynolds number $\mathrm{Re_m}$, Strouhal number St, and amplitude ratio λ. The Reynolds number $\mathrm{Re_m} = u_\mathrm{m} d_\mathrm{o}/\nu$ of the working fluid is found using the mean flow velocity u_m, the diameter of the sudden expansion d_o, and the kinematic viscosity ν at the characteristic shear rate within the shear layer with prescribed values of $\mathrm{Re_m} = 4800$ and 14400. Pulsatile flows can be described by

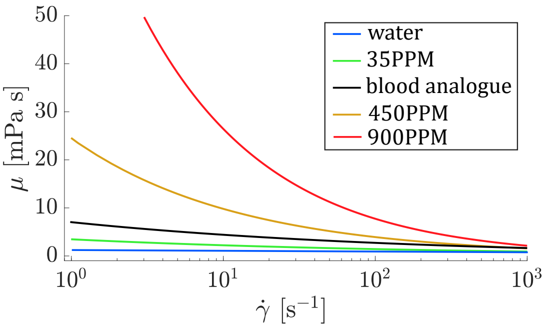

Figure 3: Viscosity strain-rate curves for all working fluids presented using power-law approximations. Increasing shear-thinning strength can be associated with decreasing flow index n. A well-known blood analogue behaviour is included from Lin *et al.* (2014) for reference.

the Strouhal number $\mathrm{St} = f d_o/u_m$ with St = 0.15 examined in this study. Chosen Re_m and St fall on the order of those found within human and large mammalian cardiovascular systems (Sundin *et al.*, 2022). The velocity program for the pulsatile cases consists of a mean flow u_m added to a sinusoid with a prescribed frequency f and amplitude u_o. Pulsatile flow cases employ an amplitude ratio of $\lambda = 0.95$, where $\lambda = u_o/u_m$.

RESULTS AND DISCUSSION

Instantaneous fields: small-scale structure attenuation

The unsteady-flow cases (St = 0.15) are dominated by shear-layer roll-up. To highlight the vortical structures and their modification with increasing shear-thinning strength, representative instantaneous normalized-enstrophy is plotted. Normalized in-plane enstrophy $\varepsilon^* = |\omega_z^2|/(u_m/d_o)^2$ is plotted for all $\mathrm{Re}_m = 4800$ cases in Figures 4a-d and for all $\mathrm{Re}_m = 14400$ cases in Figures 4e-h. Evidence of increasing anisotropic shear-layer behaviour is observed with increasing shear strength. Particularly, small-scale vortical structures are shown to attenuate with increasing shear-thinning strength. For the Re_m = 4800 cases (Figures 4c-d), increasing shear-thinning strength results in the diffusion of KH instabilities from concentrated enstrophy cores to a 'smeared' shear layer, which is analogous to the attenuation of KH instabilities in shear-thinning fluids as observed by Kumar & Homsy (1999). The number of concentrated enstrophy cores also reduces for the higher Reynolds number case, although far less pronounced, which may be indicative of self-similarity being reached for the increased turbulent flow.

An analogous instability damping is also observed within the steady shear-layer cases (St = 0). Representative instantaneous normalized-vorticity fields $\omega_z^* = \omega_z d_o/u_m$ are plotted in Figure 5 to characterize the topology and motion of vortical structures. The leftmost column of figures present Re_m = 4800, while the rightmost column of figures present Re_m = 14400, with shear-thinning strength increasing as one proceeds downwards row by row. In flows of water and 35PPM at Re_m = 4800 in Figure 5(a & c, respectively), KH instabilities shed at regular intervals and convect downstream until breakdown into turbulence. In contrast, for the Re_m = 4800 cases at 450PPM and 900PPM, concentrated vortex cores are absent and instead, vorticity is diffused into a smeared shear layer. Furthermore, two or more consecutive instabilities will commonly coalesce, resulting in the formation of large rollers convecting downstream. At the higher Reynolds number, structure coalescence is not observed and the diffusion of concentrated cores to a diffuse shear layer is present but less pronounced, again suggesting self similarity of the high Reynolds-number flow.

Unsteady & steady cases: persistence of large-scale flow-structures

Despite the attenuation of small-scale structures observed across all shear layers, the general topological features of the flows appear preserved. For the unsteady cases, the integral behaviour of the vortex roll-up is best captured by normalized phase-averaged circulation, $\langle\Gamma^*\rangle = \langle\Gamma\rangle/u_m d_o$, shown in Figure 6. For all Re_m = 4800 cases, circulation increases until roughly t/T = 0.4, coinciding with the maximum amount of rotational fluid being accepted from the shear layer. This is followed by the decay of circulation after t/T = 0.6, which coincides with the breakdown and convection of the vortex downstream. Trends in circulation are also preserved in the Re_m = 14400 cases, with Γ^* varying only slightly with shear-thinning strength with water accepting rotational fluid from the shear layer at a lower rate compared to the other fluids.

The general vortex topology revealed by instantaneous enstrophy fields, as well as the circulation trends, are shown to be generally insensitive to changes in Re_m and shear-thinning strength. This would suggest that the early formation of large-scale vortex structures is at first approximation an inviscid process. However, the smearing of vortical regions that correspond to the smaller shedding structures suggests some diffusion of initial embedded KH instabilities.

In the case of the steady shear layers, their integral behaviour can be measured using the vorticity thickness, which estimates the thickness of the shear layer. It is defined as $\delta_\omega = u_o(y/d_o = 1)/\dot{\gamma}_{\max}$ (Brown & Roshko 1974; Pereira & Pinho 2000). Time-averaged normalized vorticity thickness δ_ω/d_o is plotted to characterize the steady flow downstream of the sudden expansion for the $\mathrm{Re}_m = 4800$ cases in Figure 7a and for $\mathrm{Re}_m = 14400$ cases in Figure 7b. Results from Pereira & Pinho (2000) for shear-thinning fluid separating off a backward facing step ($\mathrm{Re}_m = 19400$ and $n = 0.43$), which is a Cartesian analogue to the axisymmetric sudden expansion studied here, are provided for comparison.

The shear layer diffusion results observed by Pereira & Pinho (2000) exhibited a spreading rate of $\mathrm{d}\delta_\omega/\mathrm{d}x \approx 0.13$. Pereira & Pinho (2000) concluded that viscoelasticity appeared to be responsible for reduced levels of turbulent kinetic energy in strongly shear-thinning cases. The steady cases presented here also exhibit a similar spreading rate, demonstrating that the integral behaviour of the shear layer is the same across all cases, despite clear temporal differences that are apparent from the steady shear-layer vorticity fields later shown in Figure 5. The result further suggests that time-averaged flow metrics cannot capture the anisotropic shear-layer behaviour. However, the 900PPM case at $\mathrm{Re}_m = 4800$ presents an outlier, shown in Figure 7a, exhibiting δ_ω/d_o that is not linear with x/d_o indicating that large-scale rollers are affecting even the time-averaged results.

Steady flows: coalescence of vortical structures

It was observed from the instantaneous vorticity fields of the low-Re steady shear-layer cases that KH instabilities were prone to coalesce while convecting downstream. This phenomena is further explored here using the normalized Reynolds-stress spectra $\Phi\, u'v'/u_m^2$, the intensities of which are plotted as color maps in Figure 8. Where u' and v' respectively represent the streamwise and vertical fluctuating velocity components and are calculated by subtracting the time-averaged velocity from the total velocity. For the spectra presented here, we limit ourselves to the velocity content sampled along a horizontal line at $y/d_o = 0.5$, which is, generally speaking, the midpoint of the shear layer. Spectral content is normalized using $d_o/2$, which is effectively a 'step height' (Poole & Escud-

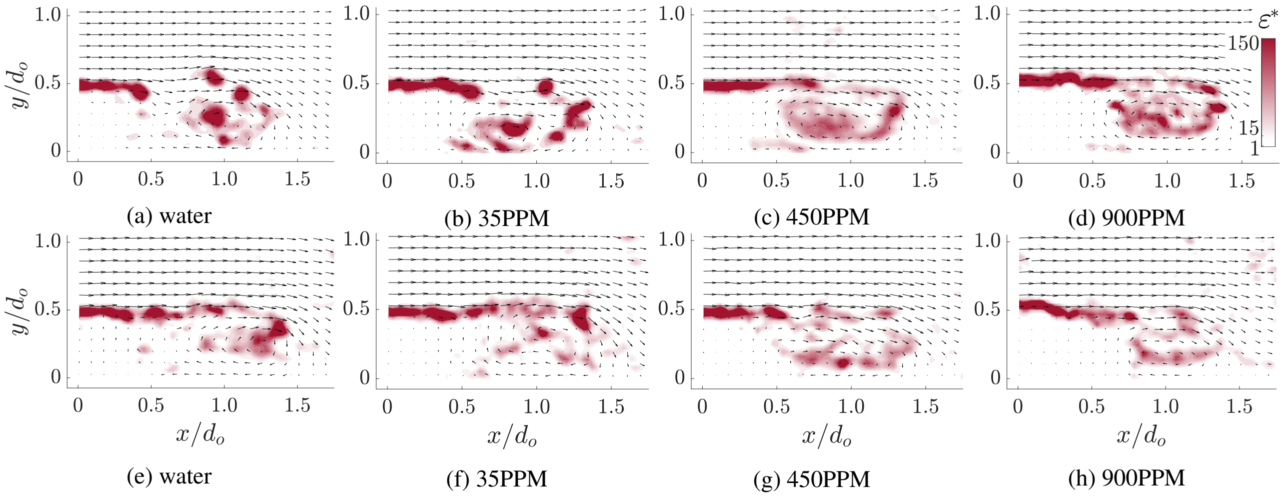

Figure 4: Representative instantaneous normalized enstrophy $\varepsilon^* = |\omega_z^2|/(u_m/d_o)^2$ and vectors plotted at $t/T = 0.25$ (top row): cases at $\mathrm{Re_m} = 4800$, and (bottom row): cases at $\mathrm{Re_m} = 14400$. All cases exhibited a frequency of St = 0.15.

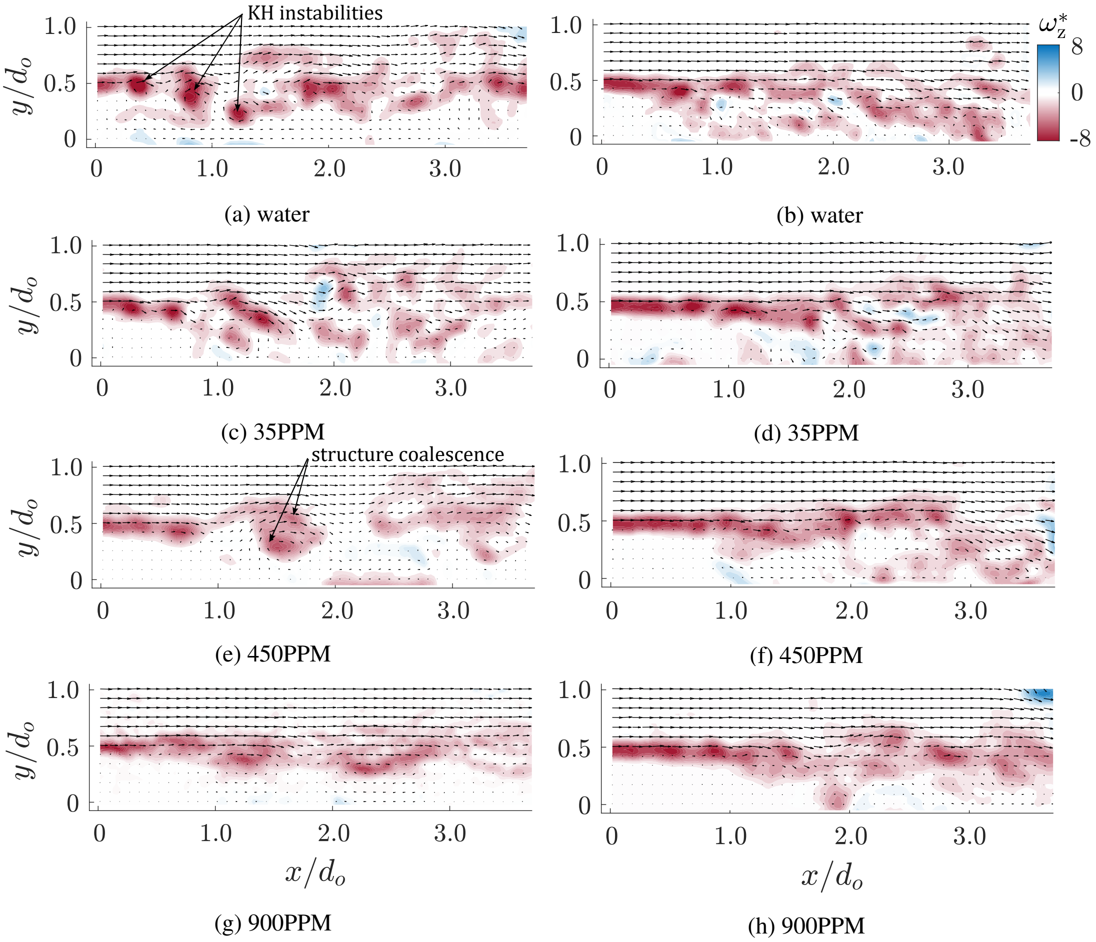

Figure 5: Representative instantaneous normalized vorticity ω_z^* and vectors for steady cases at (right): $\mathrm{Re_m} = 4800$ and (left): $\mathrm{Re_m} = 14400$. Every third vector is plotted for clarity.

ier 2004). The spectral content is shown from St = 0 to 1.15 to focus on meaningful low-frequency content. The spectral intensity along y/d_o = 0.5 is plotted against streamwise distance (x-axis) and Strouhal number (y-axis), for $\mathrm{Re_m} = 4800$ in Figures 8a-d and for $\mathrm{Re_m} = 4800$ in Figures 8e-h.

Looking to the spectral results shown in Figure 8, the regular shedding of the KH instability is indicated by the strong band of intensity at St = 0.18. This regular shedding is particularly the case for the $\mathrm{Re_m} = 4800$ cases (Figures 8a-d), but is somewhat subdued in the spectra for the $\mathrm{Re_m} = 14400$ cases (Figures 8e-h). Spectral bands of high intensity at St numbers higher than the characteristic KH shedding frequency can be attributed to the 'bursting' of small-scale structures, where bursting represents the sudden splitting of structures in to smaller structures. The bands are attributable to bursting at low x/d_o where this phenomena was observed. Harmonics of the KH shedding St are also attributed to the signals' largely monotonic behaviour and self-interaction of said dominant modes. Additionally, another small-scale structure signature exists at St = 0.62 for most cases at $\mathrm{Re_m} = 14400$.

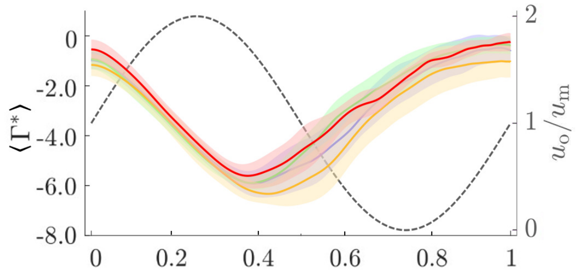

(a) $\mathrm{Re_m} = 4800$

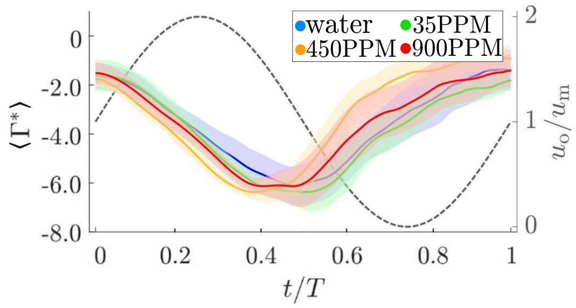

(b) $\mathrm{Re_m} = 14400$

Figure 6: Normalized phase-averaged circulation $\langle\Gamma^*\rangle = \langle\Gamma\rangle/u_m d_o$ for (top) $\mathrm{Re_m} = 4800$ and (bottom) $\mathrm{Re_m} = 14400$ over one normalized time period. The shaded regions represent one standard deviation. The prescribed incoming velocity profile u_o/u_m fluctuates sinusoidally with δ_ω/d_o as indicated by the dashed line and right axis.

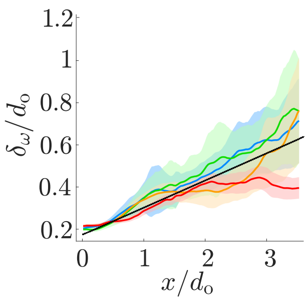

(a) $\mathrm{Re_m} = 4800$

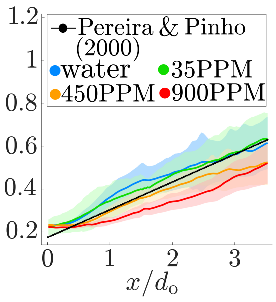

(b) $\mathrm{Re_m} = 14400$

Figure 7: Normalized vorticity thickness δ_ω/d_o for (left) $\mathrm{Re_m} = 4800$ and (right) $\mathrm{Re_m} = 14400$ for all fluids using time-averaged velocity data. Data from Pereira & Pinho (2000) ($\mathrm{Re_m}$ = 19400, $n = 0.43$) is plotted from experiments in shear-thinning backwards-facing step flows. Shaded region represents one standard deviation.

As shear-thinning strength increases, fluctuations outside of the strong structures and their harmonics are attenuated as clearly seen in the spectral content observed in Figure 8d and h. It is apparent from the spectral content of the $\mathrm{Re_m} = 4800$ cases (Figures 8a-d) that high-frequency spectral intensity reduces with increasing shear-thinning strength, which is indicative of the attenuation of small-scale structures observed here and in other studies. A similar reduction in high-frequency spectral intensity is observed within the $\mathrm{Re_m} = 14400$ cases (Figures 8e-h). The reduction is far more subdued, and speaks to level of self similarity of these flows given their high turbulence content. This observation was also made from the high-Re enstrophy fields shown in Figure 4.

Further to this regular shedding of coherent structures, with regards to the low Reynolds-number cases (Figures 8a-d), shear-layer flapping is prominent, which is indicated by low-frequency high-intensity spectra. In backwards facing step flows, shear-layer flapping is known to affect the size of the recirculating region and consequently; the fluid mixing, vorticity diffusion, and shear-layer trajectory (Ma & Schröder, 2017).

For the $\mathrm{Re_m} = 4800$ cases, and especially within the strong shear-thinning fluid cases (Figures 8c-d), the low-frequency spectral content appears to grow more intense moving further downstream, which may be attributable to the coalescence of KH instabilities into larger rollers. The general increase in low-frequency spectra content with downstream distance appears to be enhanced with increasing shear-thinning strength. This correlates with how the regularity of coalescence also increases with shear-thinning strength, as observed within the $\mathrm{Re_m} = 4800$ vorticity fields. This increase in low-frequency spectra content is not apparent within the $\mathrm{Re_m} = 14400$ cases, again speaking to the self-similarity of these flows at their increased level of turbulence. Although the spectra correlates the trends observed within the instantaneous-flow fields and reinforces the conclusion that shear-thinning strength promotes highly anisotropic behaviour within the shear layer, the causation of the coalescing of structures and the self-organization of the spectra is unclear. One potential cause could be the streamwise reorientation of xanthan-gum molecules when extended due to straining or extensional flow, and being naturally stable against perturbations that tilt them off the streamwise axis. This would effectively stratify the flow in the radial direction about the axisymmetric expansion.

CONCLUSIONS

The current study investigates the formation of steady and unsteady (St = 0.15) shear layers forming within fluids of increasing shear-thinning strength (n = 1, 0.81, 0.61 and 0.47) to characterize how the anisotropy of shear-thinning fluids affects the formation and propagation of coherent vortical structures. Based on previous studies, it was hypothesized that large-scale structure flow behaviour would be preserved while small-scale vortical structures would be damped. As such, test cases were performed at equivalent Reynolds numbers of $\mathrm{Re_m} = 4800$ and 14400 were used to account for changes in effective viscosity.

The shear layers investigated herein were generated via an axisymmetric sudden expansion. Planar PIV measurements of the tested shear layer cases were performed to extract measurements of their large-scale flow, as well as the embedded small-scale vortical structures. Measurements of large-scale flow, particularly the circulation in the unsteady cases and the vorticity thickness in steady cases, showed preservation of large-scale flow. Instantaneous enstrophy and vorticity fields for both unsteady and steady cases, respectively, demonstrated attenuation and diffusion of small-scale vortical structures from concentrated cores to smeared diffuse structures, an observation that becomes more apparent with increasing shear-thinning strength. This attenuation is especially true for the $\mathrm{Re_m}$ = 4800 cases, whereas the $\mathrm{Re_m}$ = 14400 cases exhibits more self-similarity due to increased turbulence. The conclusion that at high $\mathrm{Re_m}$ the flow behaves in an increasingly more similar manner was reinforced by the fluctuation spectra along the midpoint of the shear layer: high-frequency content reduces with increasing shear-thinning strength for $\mathrm{Re_m}$ = 4800 cases and less so for $\mathrm{Re_m}$ = 14400 cases. Finally, and especially for the low-Re cases, the coalescing of small-scale vortical structures was observed from instantaneous vorticity fields, an observation that was reinforced by the increasing of low-frequency content with increasing downstream distance.

The results align with the hypothesis and previous work, which are based on a shear-thinning fluid's tendency to preserve the large-scale flow while damping the small-scale structures through shear-layer anisotropy (Escudier *et al.*, 2009).

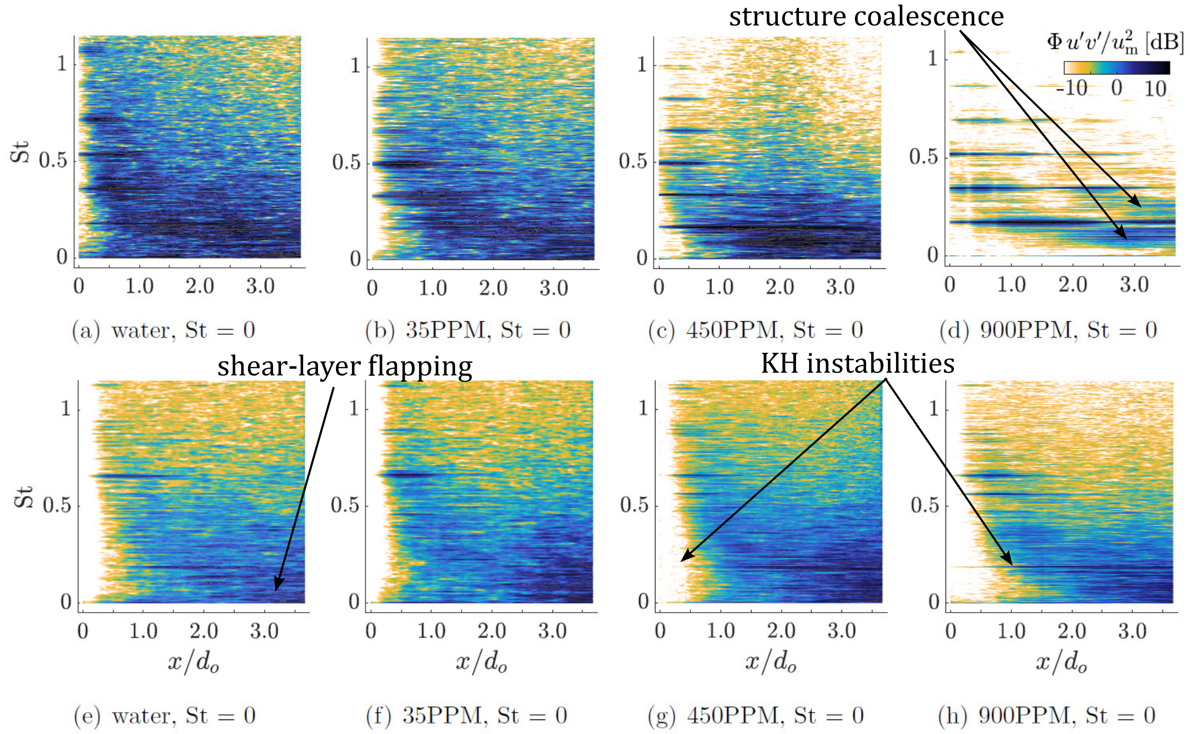

Figure 8: Normalized Reynolds stress spectra $\Phi\ u'v'/u_m^2$ presented in relative decibels for steady shear-thinning fluid flows for (top row) $\mathrm{Re_m} = 4800$ and (bottom row) $\mathrm{Re_m} = 14400$. For the $\mathrm{Re_m} = 4800$ cases, as shear-thinning strength increases, general reduction in intensity occurs across the entire spectra, with the harmonics from the shedding persisting indicating a largely monotonic signal.

However, this damping is overtaken at high Reynolds numbers, at which point turbulence promotes self-similarity of the flow. Despite the results supporting our hypothesis, the cause behind the damping and coalescing of small-scale vortical structures is unclear. It is believed that the elongation and reorientation of xanthan-gum molecules in the streamwise plane may act to stabilize the flow against fluctuations, but this prediction is left for future work.

REFERENCES

Bentata, O., Anne-Archard, D. & Brancher, P. 2018 Experimental study of low inertia vortex rings in shear-thinning fluids. *Phys. Fluids* **30**.

Brown, G. L. & Roshko, A. 1974 On density effects and large structure in turbulent mixing layers. *J. Fluid Mech.* **64** (4).

Dabiri, J.O. 2009 Optimal vortex formation as a unifying principle in biological propulsion. *Annu. Rev. Fluid Mech.* **41**.

Escudier, M.P., Nickson, A.K. & Poole, R.J. 2009 Turbulent flow of viscoelastic shear-thinning liquids through a rectangular duct: Quantification of turbulence anisotropy. *J. Non-Newton. Fluid Mech.* **160**.

Gharib, M., Rambod, E. & Shariff, K. 1998 A universal time scale for vortex ring formation. *J. Fluid Mech.* **360**.

Glezer, A. 1988 The formation of vortex rings. *Phys. Fluids* **31**.

Hussain, A.K.M.F. 1986 Coherent structures and turbulence. *J. Fluid Mech.* **173**.

Jeronimo, M. & Rival, D. 2021 On the lifespan of recirculating suspensions with pulsatile flow. *J. Fluid Mech.* **928** (A2).

Kelessidis, V., Dalamarinis, P. & Maglione, R. 2011 Experimental study and predictions of pressure losses of fluids modeled as herschel–bulkley in concentric and eccentric annuli in laminar, transitional and turbulent flows. *J. Pet. Eng.* **77** (3).

Kumar, S. & Homsy, G. 1999 Direct numerical simulation of hydrodynamic instabilities in two- and three-dimensional viscoelastic free shear layers. *J. Non-Newton. Fluid Mech.* **83** (1).

Lin, L., Walker, A. & Rival, D.E. 2014 The characterization of a non-newtonian blood analog in natural- and shear-layer-induced transitional flow. *Biorheology* **51**.

Ma, X. & Schröder, A. 2017 Analysis of flapping motion of reattaching shear layer behind a two-dimensional backward-facing step. *Phys. Fluids* **29** (11).

Mrokowska, M.M. & Krzton-Maziopa, A 2019 Viscoelastic and shear-thinning effects of aqueous exopolymer solution on disk and sphere settling. *Sci. Rep.* **9**.

Palacios-Morales, C. & Zenit, R. 2013 The formation of vortex rings in shear-thinning liquids. *J. Non-Newton. Fluid Mech.* **194**.

Pereira, A. & Pinho, F. 2000 Turbulent characteristics of shear-thinning fluids in recirculating flows. *Exp. Fluids* **28**.

Poole, R. J. & Escudier, M. P. 2004 Turbulent flow of viscoelastic liquids through an axisymmetric sudden expansion. *J. Non-Newton. Fluid Mech.* **117**.

Rahgozar, S. & Rival, D.E. 2017 On turbulence decay of a shear-thinning fluid. *Phys. Fluids* **123101** (29).

Rudman, M., Blackburn, H., Graham, L. & Pullum, L. 2004 Turbulent pipe flow of shear-thinning fluids. *J. Non-Newton. Fluid Mech.* **118** (1).

Sundin, J., Bustamante, M., Ebbers, T.and Dyverfeldt, P. & Carlhäll, C-J 2022 Turbulent Intensity of Blood Flow in the Healthy Aorta Increases With Dobutamine Stress and is Related to Cardiac Output. *Front. Physiol.* **13** (1), 11.

Terrapon, V., Dubief, Y., Moin, P., Shaqfeh, E. & Lele, S. 2004 Simulated polymer stretch in a turbulent flow using brownian dynamics. *J. Fluid Mech.* **504**.

White, C. & Mungal, M. 2008 Mechanics and prediction of turbulent drag reduction with polymer additives. *Annu. Rev. Fluid Mech.* **40**.

Zhang, K. & Rival, D.E. 2020 On the dynamics of unconfined and confined vortex rings in dense suspensions. *J. Fluid Mech.* **902** (A6).